JOURNAL OF SOLID STATE CHEMISTRY 45, 324–333 (1982)

Electron Microscopy Studies of $W_{18}O_{49}$. 1. Crystals Formed by Gaseous Reduction of WO_3

WUBESHET SAHLE

Department of Inorganic Chemistry, Arrhenius Laboratory, University of Stockholm, S-106 91 Stockholm, Sweden

Received April 22, 1982; in final form June 10, 1982

$W_{18}O_{49}$ samples were prepared by reduction of WO_3 crystals at various temperatures (at about 1170, 1270, and 1370K) by equilibration with a gaseous buffer of controlled oxygen pressure. The samples were studied by high-resolution electron microscopy. The results show that an amorphous phase is an intermediary step in the formation of $W_{18}O_{49}$. Defects are very rarely observed in as-reduced $W_{18}O_{49}$, which differs in this respect from other tungsten oxides. Apart from twinning, however, three types of extended defects have been observed occasionally, and these are interpreted and discussed.

Introduction

Tungsten trioxide loses oxygen readily under reducing conditions, and a series of lower oxides is formed. From X-ray diffraction, electron microscopy, and thermodynamic studies it has been confirmed that these oxides comprise (i) {102} and {103} crystallographic shear (*CS*) structures (*1, 2*), (ii) "tunnel" compounds containing *pentagonal columns* (PC a term introduced by Lundberg (*3*), namely, $W_{12}O_{34}$ ($WO_{2.83}$) (*4–6*) and $W_{18}O_{49}$ ($WO_{2.72}$) (*7*), and (iii) WO_2 of distorted rutile-type structure (*8*). The thermal stability and composition ranges of these phases, as well as the lattice defects in the crystals, have been reviewed elsewhere (*9, 10*).

The structure of $W_{18}O_{49}$, depicted in Fig. 1, was determined from single-crystal X-ray data by Magnéli (*7*) and has been refined recently (*11*). It can be described in terms of PCs coupled in pairs by edge-sharing component octahedra. These polyhedral groups are linked together in one direction by corner-sharing component octahedra and in the other direction via additional octahedra. Wide, empty pseudo-hexagonal tunnels are formed, running through the structure along the short *b* axis.

The crystal structure gives an O/W ratio of 2.722_2 for the ideal composition. Opinions have, however, diverged considerably concerning the extension of the homogeneity range of this phase, and the following different O/W composition intervals have been suggested, in chronological order: 2.65–2.76 (*12*), 2.654–2.765 (*13*), 2.70–2.73 (*14*), 2.64–2.71 (*15*), and 2.719–2.7224 (*16*). The last interval was obtained by precision thermogravimetric studies. Neither the X-ray powder diffraction investigation by Ekström (*17*) nor the high-resolution electron microscopy (HREM) study by Pickering and Tilley (*4*) showed evidence for a variable composition of the phase.

In a recent study of the tungsten–oxygen

0022-4596/82/150324-10$02.00/0

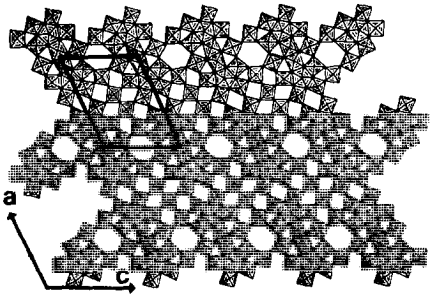

FIG. 1. Projection of $W_{18}O_{49}$ structure along the *b* axis.

system, samples of $W_{18}O_{49}$ were prepared by reduction of WO_3 crystals by equilibration with a gaseous buffer of controlled oxygen pressure (*18*). It was reported that all observed $W_{18}O_{49}$ fragments were very well ordered, except a few that contained planar faults. The effect of these faults on the composition of the phase was uncertain. On the other hand, as X-ray crystallographers have noticed, the crystals of $W_{18}O_{49}$ are frequently twinned and unsuited for single-crystal data collection (*7, 11*). A recent morphological study of the system has revealed that, although the shape of the basic WO_3 crystals was roughly preserved during the reduction, the samples of $W_{18}O_{49}$ formed consisted of compact, more or less randomly oriented bundles of needles (*19*).

Over twenty years ago Hashimoto *et al.* (*20*) studied the formation of $W_{18}O_{49}$ by thermal decomposition of ammonium tungstate in the high vacuum of a hot-stage electron microscope. They observed the occurrence of seemingly liquid, "ball-like" particles on the growing needles. Recently we found a similar feature in scanning electron microscope images at the $W_{12}O_{34}$ and $W_{18}O_{49}$ phase boundary (*19*). While coherent intergrowth was found to occur between the other structure types, no intergrowth of these two neighboring oxides has ever been observed in TEM images (*18*). It was therefore found desirable to carry out further studies on the formation of $W_{18}O_{49}$, to analyze the planar faults observed, and to throw some light on the composition variability of the oxide.

Experimental

$W_{18}O_{49}$ samples were prepared by gaseous buffer equilibration of vapor-grown tungsten trioxide crystals at about 1170, 1270, and 1370K. The purity of the initial tungsten trioxide powder was 99.9% (KOCH-LIGHT Laboratories). The details of the syntheses have been reported elsewhere (*18, 21*).

The samples were studied by optical microscopy and X-ray powder diffraction, as well as scanning, analytical, and transmission electron microscopy. A Siemens ELMISKOP 102, with a double tilt-lift stage was utilized as the main tool of investigation. For use in the microscope the samples were crushed in an agate mortar, dispersed in *n*-butanol, and collected on copper-supported perforated carbon films. Thin crystal flakes (less than 100 Å thick) were sought and oriented with [010] parallel to the electron beam. Micrographs were recorded at about 800 Å underfocus, using all diffracted beams out to about 0.42 Å; the effective size of the aperture was smaller, due to focus spread and beam convergence, however (*22*).

The oxide is stable in the beam, has two long axes and one short, and is thus very well suited for lattice imaging. To ease the interpretation of the observed faults, we made *n*-beam dynamical calculations using the multislice method (*23, 24*). These provided the basis for the interpretation of the images as a projected charge density of the crystals. For the calculations we made use of a computer program originally written by Skarnulis (*25*) and further modified at our Institute by Kihlborg.

Results and Discussion

All diffraction lines in the X-ray powder

patterns of the $W_{18}O_{49}$ samples could be indexed, and the lattice parameters were unaffected by variations in the synthesis temperature, unlike those of the other oxides. The lattice parameters observed were a = 18.322 ± 0.002, b = 3.782 ± 0.002, c = 14.034 ± 0.002 Å, and β = 115.21 ± 0.02°, and these values are in good agreement with values previously reported (*17*). We will now examine how the formation of $W_{18}O_{49}$ is accomplished during reduction of WO_3 crystals and then present the observed planar faults in the oxide.

(1) Formation of $W_{18}O_{49}$

The sequence of phases occurring during the reduction of WO_3 crystals down to $WO_{2.72}$ has been investigated recently (*18*). Fragments representing intergrowth of the four more oxidized phases were observed, but intergrowth among these and $W_{18}O_{49}$ was never seen. Observation of the samples containing $W_{12}O_{34}$ and/or $W_{18}O_{49}$ under an optical microscope frequently showed bunches of whiskers of $W_{18}O_{49}$ grown from a common center (*19*). The material in the

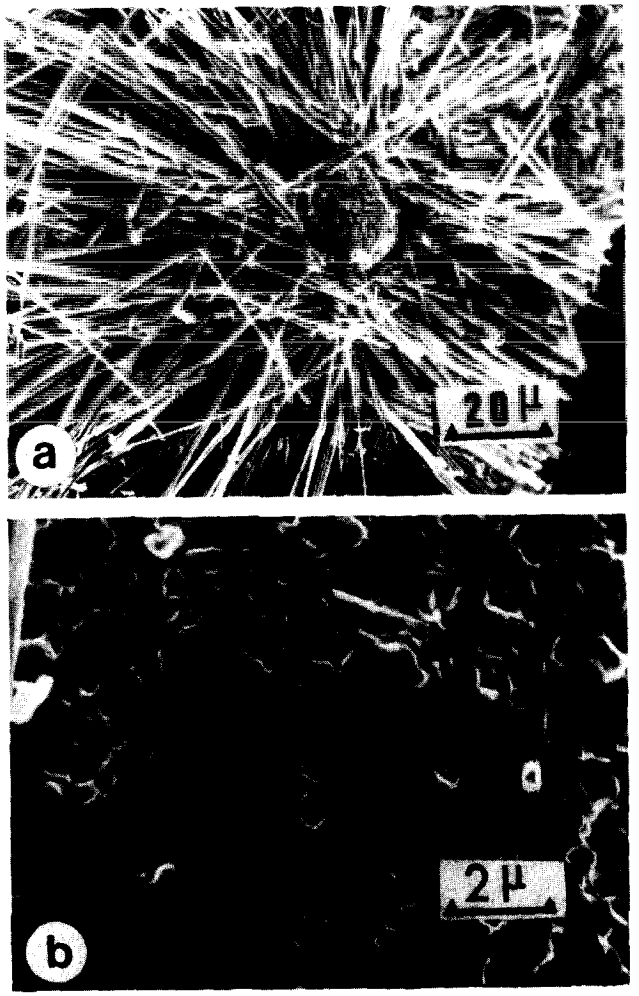

FIG. 2. (a) Formation of $W_{18}O_{49}$ whiskers in wet gaseous reduction of WO_3 crystals. (b) A SEM micrograph of amorphous tungsten oxide (higher magnification of the core in (a).

center appeared rather glassy and distinctly different from the surrounding material. Further examination of such regions, apparently nucleation centers of $W_{18}O_{49}$ whiskers, in a scanning electron microscope revealed that they consisted of ball-like particles (Fig. 2a). Higher magnification of the central part showed an appearance rather different from that of a crystalline material (Fig. 2b).

The same samples, when observed in a transmission electron microscope, showed many fragments like that in Fig. 3a, which gave only diffuse scattering in diffraction mode (Fig. 3b). Such amorphous flakes have only been seen in samples also containing $W_{12}O_{34}$ and/or $W_{18}O_{49}$. Energy-dispersive analysis indicated that tungsten was the only or main detectable element in these amorphous fragments.

These results indicate that the formation of $W_{18}O_{49}$ from the higher oxide $W_{12}O_{34}$ in these experiments is not a coherent and gradual structural transformation, but a nucleation and subsequent growth of the oxide. An amorphous tungsten oxide seems to be an intermediate stage in this process.

(2) Faults in $W_{18}O_{49}$

The HREM studies showed that the $W_{18}O_{49}$ crystals were normally well ordered, except for a few fragments in which

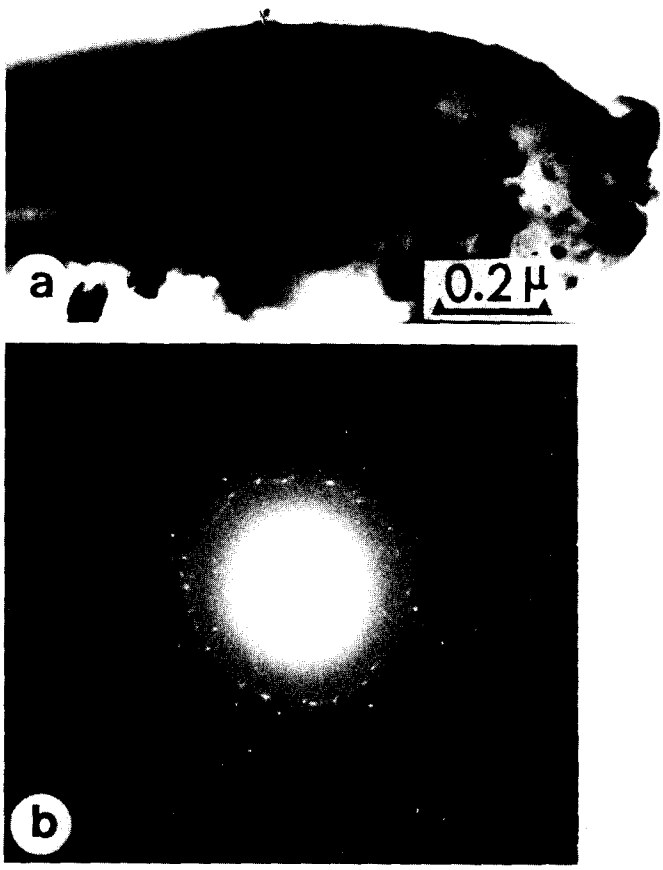

FIG. 3 (a). Transmission electron image of a predominantly amorphous fragment. (b) Electron diffraction pattern of the fragment shown in (a).

single planar faults could be seen. Fragments containing these faults were found exclusively in single-phase $W_{18}O_{49}$ samples, and such faulted fragments did not amount to more than 7% of the total number observed, i.e., 9 fragments out of 140. Although intensive studies were conducted on samples containing both $W_{18}O_{49}$ and $W_{12}O_{34}$, neither intergrowth nor defective $W_{18}O_{49}$ fragments were observed. Low-magnification images of these defects are presented in Fig. 4. The defects are often more clearly seen if the crystal is tilted rather far (a few degrees) from the ideal projection. Synthetic images of the $W_{18}O_{49}$ structure (Fig. 5) using the refined structure data (*11*) have been calculated in order to verify the intuitive interpretation of the micrographs. Even for thick crystals and moderate magnifications, the pseudohexagonal tunnels are clearly visible and can be used as clues for the defect interpretation.

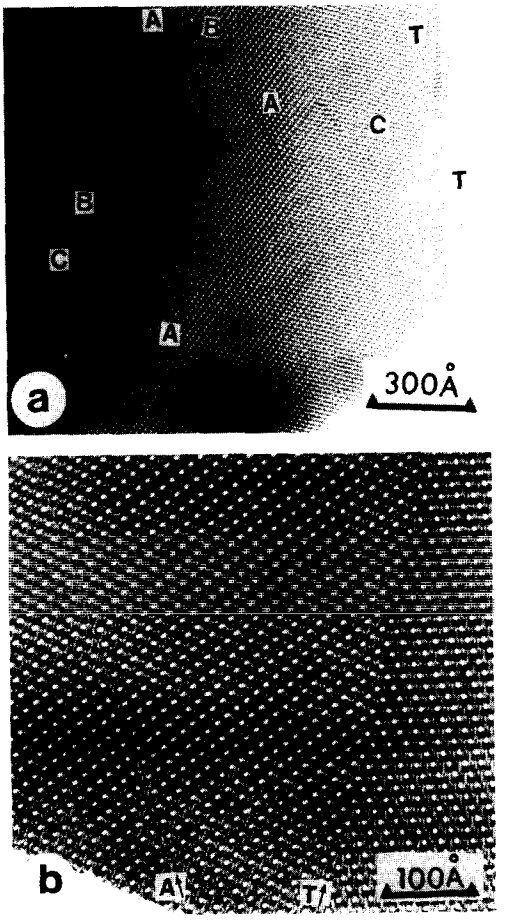

FIG. 4. (a,b) Low-magnification image of defective $W_{18}O_{49}$ crystal fragments. Defects ($\bar{1}01$) are labeled *A*, those lying on ($\bar{2}01$) are marked *B*, and others which are parallel to the *c* axis are designated *C*. The letter T indicates twinning.

The observed planar defects fall into three groups, according to their crystallographic orientations. The faults designated *A* lie on the plane ($\bar{1}01$), and those marked *B* lie on ($\bar{2}01$) with respect to the parent $W_{18}O_{49}$ lattice (Fig. 4). In Fig. 6 a high-resolution image of a fragment having defects of type *A* and *B* is presented. Enlargements of the defective regions are shown in Fig. 7. The two differently oriented defects terminate in each other at an angle of about 150°. It can be seen that the lattice on both sides of these faults is shifted perpendicular to (001) by about 4 Å. A likely interpretation of the defect region at the junction of the two types of faults is presented in Fig. 8. The defects indicated by *C* in Fig. 4a run parallel to the *c* axis and can thus be termed (100) defects. They are not easily interpreted in this rather low-magnification image, but one can see that the lattice viewed along *a* is shifted by approximately $\frac{1}{3}$ *c* (≈4 Å) across this defect, while there is very little expansion or contraction along *a*. A reasonable model is presented in Fig. 9.

The defects can conveniently be discussed in terms of the interconnection of the PCs. In regular $W_{18}O_{49}$ four types of linkages can be distinguished, which are shown in Fig. 10 (I–IV). These structure components, for convenience designated by symbols partly following the notation introduced by Lundberg (*3*), can be named: (I) edge-shared (α), (II) double corner-shared (γ), (III) PC–WO_3–PC (T_1), and (IV) PC–HT–PC (*H*). The α and γ types are immediate connections of PCs (*3*), while the

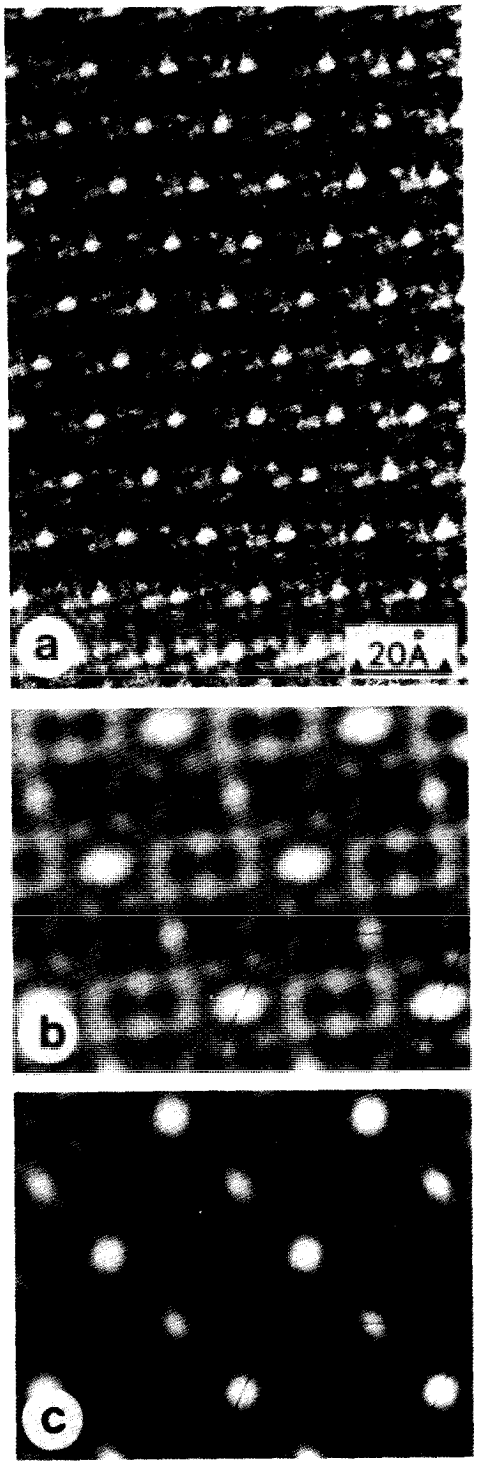

FIG. 5. Comparison of expected (synthetic) and real images of a thin, well-aligned $W_{18}O_{49}$ crystal fragment.

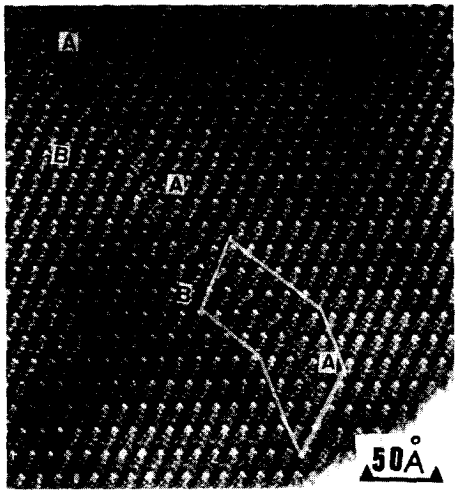

FIG. 6. Lattice image of a slightly tilted $W_{18}O_{49}$ crystal fragment, showing $(\bar{1}01)$ and $(\bar{2}01)$ defects designated *A* and *B*, respectively.

linkage occurs via extra octahedra in the *H* and *T* types. In addition, two new linkages shown in Fig. 10 (V,VI) seem to occur at the defects. These can be described as single corner-shared (δ) and PC–$(WO_3)_2$–PC (T_2) linkages.

Examination of some features along the $(\bar{1}01)$ defect (Fig. 7a, arrow) indicates that the edge-sharing between pentagonal column pairs (Fig. 10I) in $W_{18}O_{49}$ has very likely been replaced by double-corner sharing (Fig. 10II), as shown in Fig. 8. In terms of the PC joints, the α is converted to γ-linkage. At the $(\bar{1}01)$ defect there is a local increase in the number of corner-shared octahedra (WO_3-type structure), a change of T_1 to T_2, and this defect must be accompanied by an insertion of extra tungsten and oxygen atoms to the regular structure. The linkage at the defect is compared with that in regular $W_{18}O_{49}$ in Table I.

(Parameters used in the calculations: number of beams: 337; defocus: −800 Å; aperture: 0.42 $Å^{-1}$; focus spread: 150 Å; beam divergence: 1.00×10^{-3} rad; slice thickness = b = 3.78 Å.) (a) Real image; (b) synthetic image for 6 slices: (c) for 50 slices.

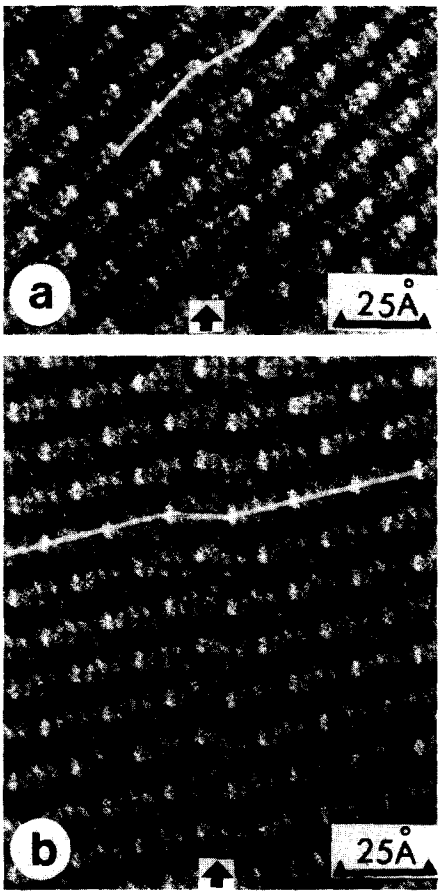

FIG. 7. (a) Enlargement of a region marked *A* in Fig. 6. (b) Enlargement of a region marked *B* in Fig. 6. (The arrow indicates the defects and the 4-Å shift of the lattice perpendicular to (001) is illustrated by the kinked lines.)

By closer inspection of the features along the $(\bar{2}01)$ defect (Fig. 7b, arrow) a model can be suggested in which PCs connected by α and γ linkages have been displaced relative to each other to become joined by γ and δ linkages, respectively. While the $(\bar{2}01)$ defect requires insertion of extra oxygen atoms, the $(\bar{1}01)$ and (100) defects involve a change in the local concentration of tungsten and oxygen atoms with a concomitant expansion of the lattice along the [102] direction. As is shown in Table I, the (100) defect could conveniently be discussed as a combination of features from the $(\bar{1}01)$ and $(\bar{2}01)$ defects. It consists of the T_2 linkage along [102] as in the $(\bar{1}01)$ defects and the δ linkage as in the $(\bar{2}01)$ defects. All these defects are rare in as-reduced $W_{18}O_{49}$, but the $(\bar{1}01)$ type is more common than the $(\bar{2}01)$ and (100) types. A striking fact, however, is that the defects are very stable in the microscope and can neither be formed nor destroyed by long time exposition to the electron beam under normal operating conditions.

As mentioned above, some thermodynamical studies have indicated the existence of a composition range for the $W_{18}O_{49}$ phase, but no structural confirmation is available. The small number of defective crystals observed in the samples make us believe that they make an insignificant contribution to any nonstoichiometry of the sample. If this phase has a homogeneity range (*16*) it is thus likely that this is caused mainly by point defects. The reason for the formation of the observed defects is not certain. Defects of these kinds can be introduced on a large scale by deliberate oxida-

TABLE I

THE STRUCTURE OF $W_{18}O_{49}$ DESCRIBED IN TERMS OF LINKAGE IN A GIVEN DIRECTION (THE CHANGE OF LINKAGE TYPE DUE TO $(\bar{1}01)$, $(\bar{2}01)$, AND (100) DEFECTS IS UNDERLINED)

Direction	$W_{18}O_{49}$	$(\bar{1}01)$ defect	$(\bar{2}01)$ defect	(100) defect
[100]	. . .αγαγαγ. . . .	. . .αγγγαγ. . . .	. . .αγαδαγ. . . and . . .αγγγαγ. . . .	. . .αγαδαγ. . . .
[102]	. .$HT_1HT_1HT_1$. .	. .$HT_1HT_2HT_1$. .	. .$HT_1\bar{H}T_1HT_1$. .	. .$HT_1HT_2HT_1$. .

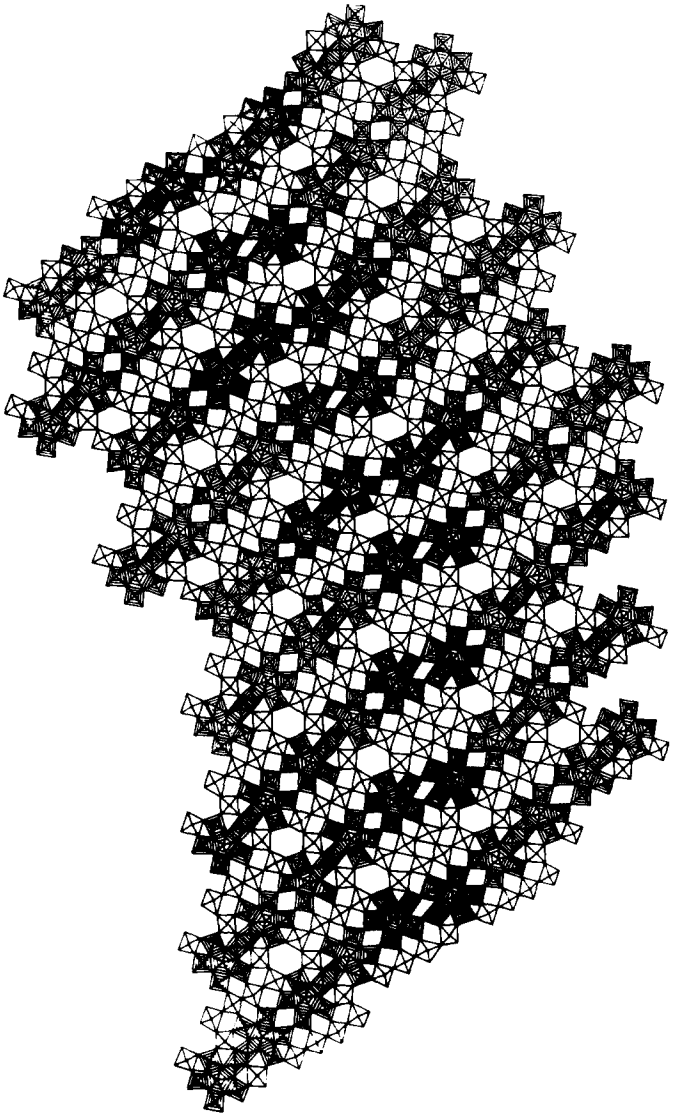

FIG. 8. Interpretation of the region in the box in Fig. 6. (The top and bottom parts of the model correspond to $(\bar{2}01)$ and $(\bar{1}01)$ defects, respectively.)

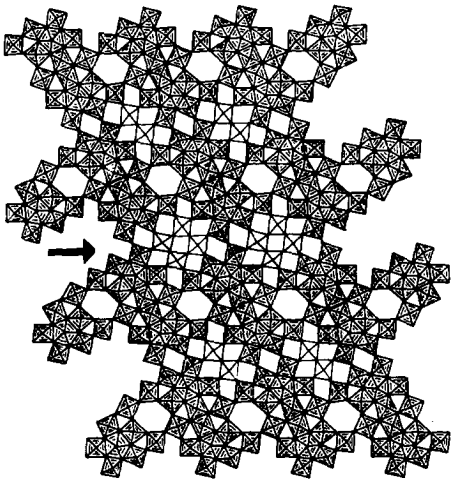

FIG. 9. An interpretation of the (100) defect marked by *C* in Fig. 4a. (The defect is indicated by an arrow.)

tion of $W_{18}O_{49}$ crystals, which will be the topic of a subsequent paper.

The conditions for the formation of the $W_{18}O_{49}$ crystals used in the present experiments were quite stable, however, and occasional oxidation does not seem likely in this case. The stability of the synthesis temperature was of the order of ±1°. The cooling was rapid; if it was not rapid enough to prevent reaction at lower temperatures, the effect would have been further reduction and not an increase in the oxygen content. It is possible that the planar defects are formed during the growth due to the presence of small amounts of impurities, perhaps present only at the nucleation center of the whiskers.

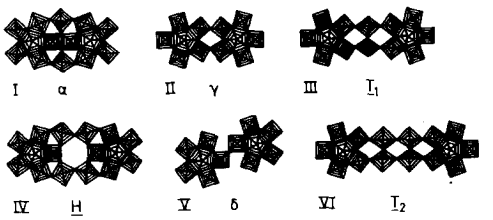

FIG. 10. The various types of PC joints in $W_{18}O_{49}$. (I) Edge-shared (α); (II) double corner-shared (γ); (III) PC–WO_3–PC (T_1); (IV) PC–HT–PC (*H*) (*26*); (V) single corner-shared (δ); and (VI) PC–$(WO_3)_2$–PC (T_2).

Acknowledgments

I am deeply indebted to Professor Lars Kihlborg for continued guidance and enthusiastic encouragement of the work and also for many stimulating discussions with him, Drs. Margareta Sundberg, and Örjan Sävborg. The preparation of many of the samples discussed in this article was based on joint work with Dr. Sven Berglund. The help of Dr. Chris Chatfield at the Coromant Research Laboratory of Sandvik AB, Stockholm, is also acknowledged with gratitude. It is a pleasure to thank Mrs. Gunvor Winlöf and Mr. Georg Kruuse for their skillful technical assistance. The study was performed within a research program supported by the Swedish Natural Science Research Council.

References

1. A. MAGNÉLI, *Ark. Kemi* **1,** 513 (1950).
2. R. J. D. TILLEY, *Mater. Res. Bull.* **5,** 813 (1970).
3. M. LUNDBERG, *Chem. Commun. Univ. Stockholm,* No. XII (1971).
4. R. PICKERING AND R. J. D. TILLEY, *J. Solid State Chem.* **16,** 247 (1976).
5. M. SUNDBERG, *Chem. Scr.* **14,** 161 (1978–79).
6. M. LUNDBERG, M. SUNDBERG, AND A. MAGNÉLI, *J. Solid State Chem.* **44,** 32 (1982).
7. A. MAGNÉLI, *Ark. Kemi* **1,** 223 (1950).
8. A. MAGNÉLI, *Ark. Kemi Mineral. Geol. A* **24,** 1 (1946).
9. "Gmelin Handbuch der anorganischen Chemie," Wolfram Erg.-Bd. B2, Springer-Verlag, Berlin/Heidelberg/New York (1979).
10. R. J. D. TILLEY, *in* "Chem. Phys. of Solids and Their Surfaces" (M. W. Roberts and J. M. Thomas, Eds.), Vol. 8, p. 121, The Chemical Society, London (1980).
11. K. VISWANATHAN, K. BRANDT, AND E. SALJE, *J. Solid State Chem.* **36,** 45 (1981).
12. O. Glemser and H. Sauer, *Z. Anorg. Allg. Chem.* **252,** 144 (1943).
13. M. P. MOROZOVA AND L. L. GUETSKINA, *Vestn. Leningr. Univ.* **22,** 128 (1952).
14. A. GULBRANSEN, K. F. ANDREW, P. E. BLACKBURN, T. P. COPAN, AND A. MERLIN, *WADC-TR* **59,** 575 (1960).

15. M. F. MARION AND C. CHOAIN-MAURIN, *Chim. Ind. (Paris)* **88,** 483 (1962).
16. J. F. MARUCCO, P. GERDANIAN, AND M. DODE, *J. Chim. Phys.* **66,** 674 (1969).
17. T. EKSTRÖM, *Chem. Commun. Univ. Stokholm,* No. VII (1975).
18. S. BERGLUND AND W. SAHLE, *J. Solid State Chem.* **36,** 66 (1981).
19. W. SAHLE AND S. BERGLUND, *J. Less-Common Met.* **79,** 271 (1981).
20. H. HASHIMOTO, K. TANAKA, K. KOBAYASHI, S. SHIMADZU, AND M. MANNAMI, "Proceedings, 4th International Conference on Electron Microscopy, Berlin, 1958," Vol. 1, p. 447, Springer, Berlin (1960).
21. S. BERGLUND, *Chem. Scr.* **18,** 73 (1981).
22. M. A. O'KEEFFE AND J. V. SANDERS, *Acta Crystallogr. Sect. A* **31,** 307 (1975).
23. J. M. COWLEY AND A. F. MOODIE, *Acta Crystallogr.* **10,** 609 (1957).
24. P. GOODMAN AND A. F. MOODIE, *Acta Crystallogr. Sect. A* **30,** 280 (1974).
25. A. J. SKARNULIS, Ph.D. thesis, Arizona State University (1976).
26. W. SAHLE AND M. SUNDBERG, *Chem. Scr.* **16,** 163 (1980).